AIAA JOURNAL
Vol. 47, No. 2, February 2009

Improvement of Delayed–Detached Eddy Simulation Applied to Separated Flow Over Missile Fin

Jacques Riou,* Eric Garnier,† and Sébastien Deck‡
ONERA, 92190 Meudon, France
and
Claude Basdevant§
Institut Galilée, Université Paris 13, 93430 Villetaneuse, France

DOI: 10.2514/1.37742

This paper presents computational simulations of the flow over a 50-deg sweep missile fin for an angle of attack equal to 25 deg. For such an angle of attack, the flow is expected to fully separate. Nevertheless, Reynolds-averaged Navier–Stokes computations still predict the presence of a leading-edge vortex. Then, hybrid Reynolds-averaged Navier–Stokes/large eddy simulation methods are assessed. In particular, this study focuses on the delayed–detached eddy simulation and on a proposed extension of this method (EDDES), in which the objective is to accelerate the destruction of the eddy viscosity in large eddy simulation regions. These two methods are assessed in the case of a boundary-layer flow, and it is shown that the extended delayed–detached eddy simulation behaves as the delayed–detached eddy simulation method. Nevertheless, in the case of a fully separated flow downstream from a backward facing step, the resolved fluctuations obtained with the extended delayed–detached eddy simulation method are in better agreement with the experimental data than those of the delayed–detached eddy simulation computation. Finally, these two methods improve the description of the flow over the missile fin, predicting a fully separated flow. However, the extended delayed–detached eddy simulation ensures a faster development of instabilities than the delayed–detached eddy simulation and the agreement with the pressure distribution obtained with pressure sensitive paint is much better with the proposed modification of delayed–detached eddy simulation.

Nomenclature

b	=	span length
C_D	=	drag coefficient
C_L	=	lift coefficient
c	=	root chord of fin
$G(f)$	=	spectral power density
K_p	=	coefficient of pressure
M_∞	=	freestream Mach number
Re_c	=	Reynolds number
St_c	=	Strouhal number
U_∞	=	freestream velocity
u, v, w	=	time-averaged velocities
υ_t	=	eddy viscosity
x_c	=	longitudinal location
x_{cp}	=	longitudinal position of the aerodynamic center of pressure
α	=	angle of attack
Λ	=	sweep angle

I. Introduction

FROM an industrial point of view, an accurate prediction of normal force and pitching moment on missile fins is essential to minimize both the fin surface and the fin actuator power consumption. These quantities are easily predictable in the supersonic regime but former attempts performed at ONERA with Reynolds-averaged Navier–Stokes (RANS) computations in the transonic regime have demonstrated that classical one- or two-equation models significantly overestimate the lift with respect to experiments from moderate to high angles of attack. The missile fin studied in this paper can be identified to a 50-deg swept delta wing. The flow over such wings is a recent topic of interest mostly because of its application to an unmanned combat air vehicle. Nevertheless, the literature concerning flows over a moderate sweep angle delta wing ($45 \text{ deg} \leq \Lambda \leq 55 \text{ deg}$) is much scarcer than the one dedicated to high sweep angle wings which have been the subject of many experimental [1–4], numerical [5–10], and theoretical [11,12] studies.

A reduction of the sweep angle with respect to the high sweep angle situation results in the following modifications of the flow. The interaction between the second vortex and the separated shear layer entails the generation of two vortices of the same sign of vorticity [13–15]. The vortex breakdown occurs at a smaller angle of attack [16]. Once it has reached the apex of the wing, the shear layer emanating from the leading edge elongates and lifts from the surface of the wing. As the angle of attack is further increased, the shear layer fails to reattach on the wing and the flow is then fully separated [17–19].

Furthermore, whatever the sweep angle of the delta wing, unsteady [20–22] and steady [23–25] vortical structures are observed in the free shear layer emanating from the leading edge of the wing.

Some data highlighting the specificity of the transonic flows with respect to subsonic ones can be found in the literature. When increasing the Mach number, the shape of the primary vortex is modified [26]. Furthermore, investigations over delta wings [27–33] reveal the occurrence of crossflow shock and rear shock waves which may enhance the separation of the second vortex and can interact with the vortex breakdown.

Additionally, convective Mach numbers near 0.6 are found in the computation of the transonic flow over the present missile fin. It has been highlighted that such compressibility effects may be strong

Received 27 March 2008; revision received 22 October 2008; accepted for publication 25 October 2008.

*Ph.D. Student, Applied Aerodynamics Department, 8 rue des Vertugadins; jacques.riou@onera.fr.
†Research Engineer, Applied Aerodynamics Department, 8 rue des Vertugadins; eric.garnier@onera.fr.
‡Research Engineer, Applied Aerodynamics Department, 8 rue des Vertugadins; sebastien.deck@onera.fr.
§Professor, Laboratoire Analyse, Géométrie et Applications, 99 avenue J. B. Clément; Basdevan@math.univ-paris13.fr.

enough to decrease the growth rate of a shear layer [34–37]. The increase of the Mach number can also result in a more significant decrease of the two Reynolds stress components $\overline{v'^2}$ and $\overline{w'^2}$ in comparison with $\overline{u'^2}$, leading to an anisotropic flow [38,39]. Finally, the shape of the vortical structures embedded in the shear layer is altered and becomes more three dimensional [40,41].

On the numerical side, it has been demonstrated that direct numerical simulation [42–45] or large eddy simulation (LES) [46] of the flow over moderate to high sweep delta wing at low to moderate Reynolds numbers provided a satisfying description of these phenomena. However, the Reynolds number of the present study involving wall-bounded flows makes use of such numerical methods impossible with the currently available computational power.

Conversely, RANS computations, for which the turbulence fluctuations are fully modeled, have been carried out in order to evaluate their ability to capture the aforementioned phenomena. Both steady RANS computations of Gordnier [47], Brandsma et al. [48], and unsteady RANS computations performed by Morton et al. [49,50] underlined the fact that an excessive amount of eddy viscosity in the rotational flow resulted in the failure of these computations in describing the main features of the flow over slender delta wings.

Hybrid RANS/LES approaches [51] represent a credible alternative to improve the description of such flows at a reasonable cost by taking into account most of the flow unsteadiness. The main idea of these methods is to model the turbulent structures in the attached region of the flow and to solve the large length-scale structures elsewhere. One of the most popular RANS/LES methods is detached eddy simulation (DES) [52] proposed by Spalart et al. A major issue in the use of the original approach is the existence of a gray area between the RANS and LES regions whose location depends only on grid spacing. Problems arise when this gray area penetrates into the boundary layer which can lead to unphysical outcomes such as modeled stress depletion. To overcome this drawback, two extensions of the original method, namely, zonal DES (ZDES) [53] and delayed DES (DDES) [54] can be used. The DDES approach is retained for this study. As this latter approach is recent and thus still in development, the separated flow over a missile fin is a good test case to assess a new extension of DDES termed extended DDES (EDDES) which is proposed in this paper. By changing the formulation of the length scale and the wall-correction functions when the DES operates in LES mode (similar to ZDES), the EDDES permits a faster decay of the level of turbulent viscosity. The latter should allow for a quick generation of resolved fluctuation in the shear layer. Having at our disposal RANS, DDES, and the new EDDES methods, the purpose of this paper is to assess the possible gain offered by the RANS/LES approaches with respect to the RANS technique currently employed in the industry.

This paper is organized as follows. For the first time, the turbulence models used in the present study are briefly presented. Especially, the newly developed EDDES is described in detail. Section II is dedicated to the validation of the EDDES method on a boundary-layer flow. Comparisons with RANS, DES, and DDES are provided. Section III reports on the comparisons between EDDES and DDES on the case of a backward-facing step flow. Finally, Sec. IV is devoted to the analysis of the separated flow over the missile fin. It includes a grid convergence study performed using RANS computations. The RANS computation carried out on the finest grid is then taken as a reference to judge the gain provided with the DDES and EDDES computations. These methods are later compared considering successively the analysis of instantaneous flows, time-averaged flows, aerodynamic coefficients, and turbulence spectra.

II. Numerical Method

A. FLU3M Solver

All the computations presented in this paper have been performed using the FLU3M solver [55], developed by ONERA. This code solves the compressible Navier–Stokes equations on multiblock structured grids.

The second-order Roe scheme [56] is used for the discretization of the Euler fluxes. Harten's correction [57] (set by the coefficient Ψ) is employed to prevent any violation of the second thermodynamic principle. Moreover, to ensure the stability of the computation in regions of flow discontinuities, slope limiters of minmod and Koren [58] are associated with the Roe scheme. The set of equations is advanced in time using the second-order accurate backward implicit scheme of Gear [59]. Moreover, four subiterations are used in the Newton integration.

The accuracy of the solver for DNS, LES, and hybrid RANS/LES has been assessed in various applications including flows around a two-dimensional airfoil in near stall conditions [60], afterbody flows [61–63], cavity flows [64], and synthetic jets in a crossflow [65,66].

B. Spalart–Allmaras Model

The Spalart–Allmaras one-equation model [67] solves a single evolution equation for a variable $\tilde{\upsilon}$ which is related to the turbulent viscosity. For compressible flows, a possible extension of the original model is given by [68,69]

$$\frac{\mathrm{D}\bar{\rho}\,\tilde{\upsilon}}{\mathrm{D}t} = c_{b1}\tilde{S}\,\bar{\rho}\,\tilde{\upsilon} + \frac{1}{\sigma}\left(\frac{\partial}{\partial x_j}(\mu + \bar{\rho}\,\tilde{\upsilon})\frac{\partial \tilde{\upsilon}}{\partial x_j} + c_{b2}\frac{\partial \tilde{\upsilon}}{\partial x_j}\frac{\partial \bar{\rho}\,\tilde{\upsilon}}{\partial x_j}\right) - \bar{\rho}c_{\omega 1}f_\omega\left(\frac{\tilde{\upsilon}}{d_w}\right)^2 \tag{1}$$

The turbulent viscosity is then given by

$$\mu_t = \bar{\rho}\,\tilde{\upsilon}\,f_{\upsilon 1} = \bar{\rho}\upsilon_t, \qquad f_{\upsilon 1} = \frac{\chi^3}{\chi^3 + c_{\upsilon 1}^3}, \qquad \chi \equiv \frac{\tilde{\upsilon}}{\upsilon} \tag{2}$$

where $\bar{\rho}$ denotes the Reynolds averaged density.

$\tilde{S}$ is the modified vorticity:

$$\tilde{S} = Sf_{\upsilon 3} + \frac{\tilde{\upsilon}}{\kappa^2 d_w^2}f_{\upsilon 2}, \qquad S = \sqrt{2\Omega_{ij}\Omega_{ij}}$$
$$f_{\upsilon 2} = 1 - \frac{\chi}{1 + \chi f_{\upsilon 1}}, \qquad f_{\upsilon 3} = 1 \tag{3}$$

where d_w is the distance to the closest wall. The wall destruction function f_ω is given by

$$f_\omega = g\left[\frac{1 + c_{\omega 3}^6}{g^6 + c_{\omega 3}^6}\right]^{\frac{1}{6}}, \qquad g = r + c_{\omega 2}(r^6 - r), \qquad r \equiv \frac{\tilde{\upsilon}}{\tilde{S}\kappa^2 d_w^2} \tag{4}$$

The model coefficients are

$$b_1 = 0.1355 \qquad \sigma = \frac{2}{3} \qquad c_{b2} = 0.622 \qquad \kappa = 0.41$$
$$c_{\omega 1} = \frac{c_{b1}}{\kappa^2} + \frac{1 + c_{b2}}{\sigma} \qquad c_{\omega 2} = 0.3 \qquad c_{\omega 3} = 2 \qquad c_{\upsilon 1} = 7.1$$

C. Global Hybrid RANS/LES Methods

1. Detached Eddy Simulation

The original hybrid RANS/LES method based on the Spalart–Allmaras model is the detached eddy simulation [52] (termed in the following as DES97) and was proposed to address the challenge of high Reynolds number massively separated flows.

As emphasized by Travin et al. [70], DES97 uses a single turbulent model which functions as a subgrid scale model in detached flows and as a Reynolds averaged model in attached flow regions.

Equation (1) shows that when the production and destruction terms are balanced, the model adjusts the pseudoeddy viscosity to scale with the local deformation rate as follows:

$$\tilde{\upsilon} \sim \tilde{S}d_w^2 \tag{5}$$

The DES97 method lies on a new length scale $\tilde{d}$ in replacement of d_w given by the following expression:

$$\tilde{d} = \min(d_w, C_{\mathrm{DES}}\Delta_1) \tag{6}$$

where C_{DES} is a calibrated constant equal to 0.65, and Δ_1 is the grid spacing defined by

$$\Delta_1 = \max(\Delta x, \Delta y, \Delta z) \tag{7}$$

Thus, when $d_w < C_{\mathrm{DES}}\Delta_1$, $\tilde{d} = d_w$ and the simulation operates in RANS mode. Oppositely, when $d_w > C_{\mathrm{DES}}\Delta_1$, $\tilde{\upsilon} \propto \tilde{S}\Delta_1^2$, and the model adopts the form of Smagorinsky's subgrid scale model [71].

DES was used by Görtz [72–74] to compute the flow over a 70 deg delta wing at $\alpha = 27$ deg. In spite of a relatively coarse grid, frequencies associated with the helical mode and Kelvin–Helmholtz instabilities were accurately predicted using DES. Moreover, Mitchell et al. [75] used this method to compute the flow over the same delta wing as Görtz. This computation predicts correctly the steady vortical substructures in the shear layer which have been previously observed experimentally [76].

However, in the case of an "ambiguous" density grid (i.e., the gray area penetrates into the turbulent boundary layer), this method suffers from some identified drawbacks. In particular, a premature switch to the LES mode can occur in the attached part of the flow. This results in an underestimation of the Reynolds stresses (modeled stress depletion) and possibly in a numerical separation, the latter problem being known as grid induced separation [77]. To avoid these difficulties, two main methods were derived from DES97, the ZDES [53,78] and the DDES [54]. Within ZDES, the RANS mode is explicitly imposed in selected regions where an attached turbulent boundary layer is expected. In the second approach, a modification of the length scale delays the switch into the LES mode. The DDES, which constitutes the basis of the new EDDES, is presented in the following.

2. *DDES Method*

DDES is a variant of DES97 designed to ensure that attached boundary layers are treated in RANS whatever the grid resolution. DDES uses the quantity:

$$r_d = \frac{\upsilon_t + \upsilon}{\sqrt{U_{i,j}U_{i,j}}\kappa^2 d_w^2} \tag{8}$$

where $U_{i,j}$ is the velocity gradient.

r_d is equal to 1 in the logarithmic layer and vanishes at the edge of the boundary layer and is used in the function:

$$f_a = 1 - \tanh([8r_d]^3) \tag{9}$$

which equals 0 in the boundary layer and 1 elsewhere.

The length scale $\tilde{d}$ is modified to be a function of f_a and is now defined by

$$\tilde{d} = d_w - f_a \max(0, d_w - C_{\mathrm{DES}}\Delta) \tag{10}$$

with $\Delta = \Delta_1$ in the DDES formulation.

In practice, $\tilde{d}$ equals d_w (as in RANS) in boundary layers and elsewhere, $\tilde{d} = \min(d_w, C_{\mathrm{DES}}\Delta_1)$ as in the classical DES97. f_a delays the premature switch into the LES mode and ensures that boundary layers are fully treated in the RANS mode.

This numerical method has been recently successfully applied to predict the supersonic inlet buzz [79].

3. *Extended DDES*

The ability of a hybrid RANS/LES method to develop rapidly turbulent structures is an essential feature. Unfortunately, DDES, similar to DES97, on typical grids does not achieve transition very fast (see [80]). Conversely, ZDES switches very fast to the LES mode thus limiting the extent of the gray area responsible in the delay of formation of the instabilities. The formulation of ZDES differs from those of DDES and DES97 because the near-wall functions of the RANS model are explicitly disabled in the LES mode and the length scale is given by the cube root of the cell (denoted Δ_2) analogous to classical subgrid models (see also Breuer et al. [81]).

The first proposal to overcome this drawback of DDES using length scales Δ_1 and Δ_2 in preestablished zones can be found in [82].

The idea of the proposed EDDES is to combine the above features of ZDES with the f_a limiter and is thus more general because the switch from one length scale to another is performed automatically.

In practice, the length scale Δ and the functions $f_{\upsilon 1}, f_{\upsilon 2}$, and f_ω of the Spalart–Allmaras model become functions of the quantity f_a. The behavior of these quantities now depends on the value of f_a with respect to a threshold f_{a0} which marks the border of the boundary layer.

If $f_a < f_{a0}$, then

$$\begin{cases} \Delta = \Delta_1 = \max(\Delta x, \Delta y, \Delta z) \\ f_{\upsilon 1}, f_{\upsilon 2}, \quad \text{and} \quad f_\omega \text{ are unchanged w.r.t. DES97} \end{cases} \tag{11}$$

and when $f_a \geq f_{a0}$,

$$\begin{cases} \Delta = \Delta_2 = \sqrt[3]{\Delta x \times \Delta y \times \Delta z} \\ f_{\upsilon 1} = 1 \\ f_{\upsilon 2} = 0 \\ f_\omega = 1 \end{cases} \quad \text{as in ZDES} \tag{12}$$

In Eqs. (11) and (12), f_{a0} is a user-defined value of f_a within the range (0.75, 0.99). Its value corresponds to the value at the edge of the boundary layer and has been determined on tests in a flat plate boundary layer. In the following simulations, f_{a0} has been fixed to 0.8.

Moreover, it is worthwhile to notice that the behavior of the function f_a is unchanged with respect to the classical DDES. This means that in boundary layers the EDDES behaves as classical DDES and conserves its insensitivity to the modeled stress depletion (MSD).

Outside of the boundary layer, the objective is to switch as quickly as possible toward a true LES. Subsequently, the classical LES definition of the filter length scale is adopted and wall-correction functions $f_{\upsilon 1}, f_{\upsilon 2}$, and f_ω are set to their asymptotic values far from the wall. The practical consequence of these modifications is a faster decay of the eddy viscosity in the LES mode with respect to classical DDES. Indeed, following Eq. (5), the pseudoeddy viscosity in the LES region is given by $\tilde{\upsilon} \sim \tilde{S}\Delta_1^2$ for the DDES and $\tilde{\upsilon} \sim \tilde{S}\Delta_2^2$ for the EDDES. For a classical LES grid, Δ_1 being lower or equal to Δ_2, the eddy viscosity becomes lower in the EDDES formulation than in the DDES one.

III. Validation of the EDDES in the Case of a Boundary-Layer Flow

To evaluate the EDDES method in the case of an attached flow, simulations of the flow over a flat plate without pressure gradient have been carried out. EDDES results are compared to a RANS computation (using the Spalart–Allmaras model, denoted RANS_SA) and a DDES computation. Furthermore, to illustrate the problem of MSD, results of a DES97 computation are also plotted.

The freestream velocity is $U_\infty = 226.5\ \mathrm{m \cdot s^{-1}}$, the length of the plate is $L = 0.285$ m, and the Reynolds number is $Re_L = 5.8 \times 10^6$. A three-dimensional ambiguous grid has been constructed. The grid resolution in the plane parallel to the wall ($\Delta x^+ = 200$ and $\Delta z^+ = 100$) ranges between classical values used in LES and in RANS. Figure 1 illustrates the evolution of the ratio of the eddy viscosity over the molecular viscosity in the boundary layer for a station at $x/L = 0.9$.

At the examination of this figure, it is striking to observe that DES97 does not reproduce the same level of eddy viscosity as the RANS computation which should be taken as a reference on this attached boundary-layer flow. On this grid, the switch from the

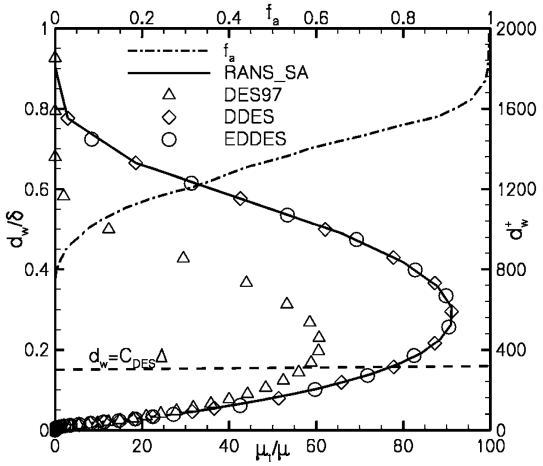

Fig. 1 Evolution of the eddy viscosity as a function of the distance to the wall.

RANS mode to the LES mode occurs at $d_w = C_{\mathrm{DES}}\Delta = 0.18\delta$, which corresponds to $d_w^+ = 300$. As a result, the maximum of μ_t/μ of the DES97 computation is underestimated by about 30% with respect to the RANS computation. This induces the modeled stress depletion shown in Fig. 2.

This figure illustrates the consequence of the early switch to the LES mode on the Reynolds cross correlation $\overline{u'v'}/u_\tau^2$. The maximum of the modeled stress $\overline{u'v'}/u_\tau^2$ is underestimated by about 25% with respect to the RANS computation at $d_w^+ = 100$. As the distance from the wall increases, the modeled stress obtained, thanks to the DES97 computation, decreases too quickly and the maximum discrepancy with the RANS computation reaches its maximum at $d_w/\delta = 0.2$, where the relative error becomes as high as 80%. Oppositely, levels of eddy viscosity and of Reynolds stress given by both DDES and EDDES equal the RANS ones. This validates the behavior of the EDDES method in the case of an attached flow.

With regard to these results, the threshold value f_{d0} is fixed equal to 0.8 for the following computations.

IV. Comparison of the DDES and EDDES Methods in the Case of a Fully Separated Flow

Once the behavior of the EDDES method is validated in the case of a boundary-layer flow, the objective is to demonstrate its competitive advantage over the DDES in the case of a fully separated flow. The chosen test case is a channel flow separating downstream from a backward-facing step (see Fig. 3). This configuration, which represents the A3C (a joint action aimed at the development of a three-dimensional code for combustion chamber modeling) combustion chamber, has been experimentally used to study the separation of inert and reactive flows downstream from the step [83–85].

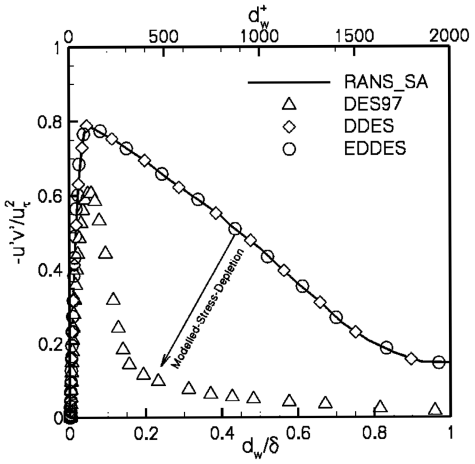

Fig. 2 Evolution of the Reynolds stress as a function of the distance to the wall.

The lateral dimension of the computational domain and the distance from the step to the outflow have been fixed by Sainte-Rose et al. [86]. The extent of the domain upstream of the step equals 34 h to ensure a boundary-layer thickness of 13 mm at the separation point.

The inlet state is defined by a main flow velocity equal to 50 $\mathrm{m \cdot s^{-1}}$ and a temperature of 520 K. Moreover, the outlet pressure is imposed equal to 100,400 Pa. Finally, a no-slip adiabatic condition is applied to the walls.

The numbers of points in the longitudinal, transverse, and normal directions are, respectively, 830, 136, and 36, ensuring a LES resolution. Moreover, particular attention has been paid to the shear layer region discretization to ensure a satisfying development of the vortical structures. More details on the mesh can be found in [85].

Turbulent structures can be underlined by plotting an isosurface of the Q criterion defined as follows [87]:

$$Q = -\tfrac{1}{2}(S_{ij}S_{ij} - \Omega_{ij}\Omega_{ij}) \tag{13}$$

where S and Ω denote, respectively, the strain of rate and rotation tensors. This quantity is useful to highlight the flow regions where the turbulence is resolved. An isosurface of $Q = h^2/2U_\infty^2$ is represented in Fig. 4 for the DDES and EDDES computations.

This figure clearly illustrates the effect of the EDDES formulation on the instantaneous flow in comparison with the DDES one. Just downstream from the step, a two-dimensional roller can be observed in the two computations. Nevertheless, in the EDDES computation, this 2-D roller quickly destabilizes into three-dimensional structures whereas a distance of 1 h is necessary to see the appearance of another big roller in the DDES instantaneous flow. Furthermore, the vortical structures are much finer and numerous in the EDDES computation than in the DDES one. Moreover, more turbulent structures are resolved in the backflow using the EDDES formulation. All of these observations suggest that there is more resolved turbulence in the EDDES computation than in the DDES one.

Figure 5 shows the evolution of the time-averaged longitudinal velocity at $x/h = 1.2$ and $x/h = 4.5$. The first station corresponds to the early development of the instabilities, whereas the second one is located just upstream of the reattachment point.

One can observe at the first location that EDDES computation is in quite good agreement with the experimental data in spite of a limited overestimation of the reverse flow. Moreover, the topology of the flow predicted by the DDES method is quite different because the intensity of the reverse flow is, for the first time, underestimated for y lower than -0.02 and then overestimated for y from -0.02 to -0.01. This different evolution of the vertical velocity gradient may alter the stability of the shear layer and then the development of the turbulent structures. At $x/h = 4.5$, the EDDES computation still satisfyingly predicts the evolution of the longitudinal velocity, whereas the DDES method significantly overestimates the intensity of the reverse flow for y lower than 0.01.

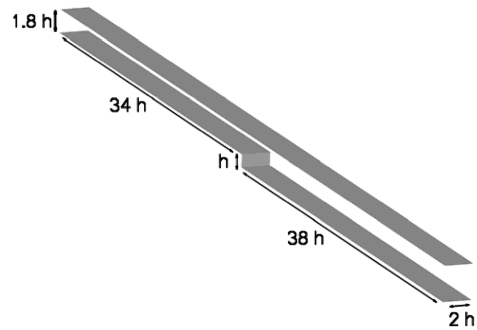

Fig. 3 Geometry of the backward-facing step and dimensions of the computational domain.

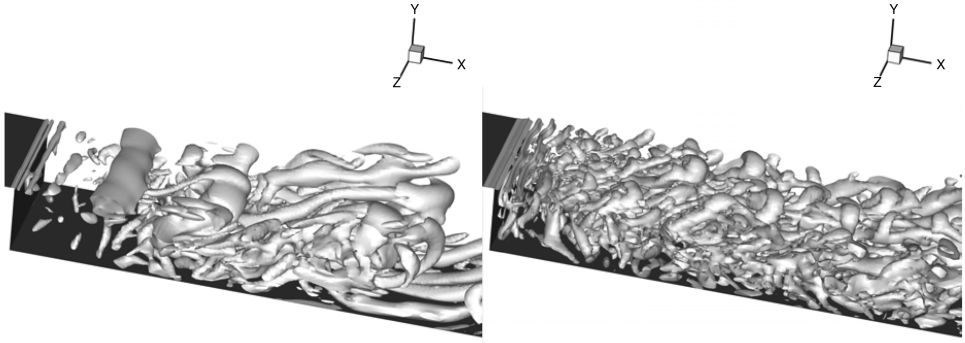

Fig. 4 Isosurface of $Q = U_\infty^2/2h^2$ highlighting the turbulent structures. Left: DDES; right: EDDES.

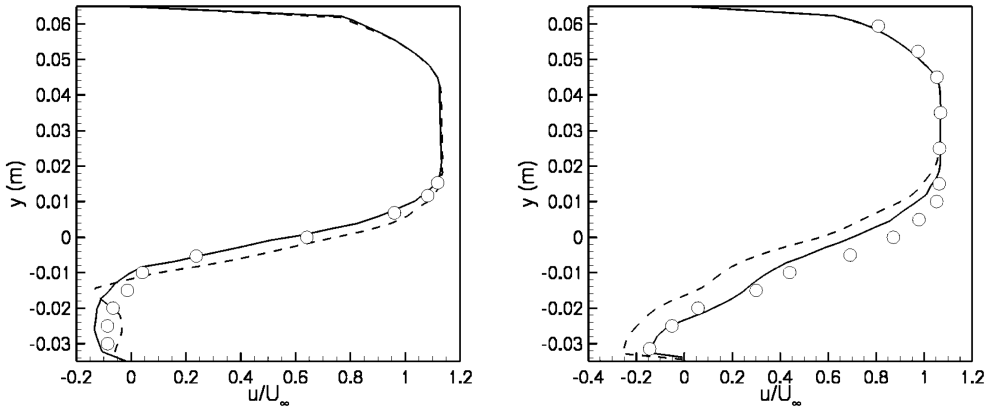

Fig. 5 Evolution of the time-averaged longitudinal velocity as a function of d_w. Left: $x/h = 1.2$; right: $x/h = 4.5$; dashed lines: DDES; solid lines: EDDES; symbols: experiment.

Figure 6 represents the evolution of the eddy viscosity at $x/h = 1.2$ and $x/h = 4.5$.

Downstream from the backward-facing step, the flow fully separates. At $x/h = 1.2$ and for y lower than 0, in the region of the reverse flow, the function f_a quickly reaches its threshold value of 0.8, resulting in a decrease of the eddy viscosity in the EDDES computation. This decay of μ_t is particularly strong in the region of the shear layer, between $y = 0$ and $y = 0.006$ m, with the eddy viscosity being divided by 4 with respect to the DDES computation. It should be noted that the excess eddy viscosity present in the DDES computation between $y = 0.006$ and $y = 0.025$ is caused by the eddy viscosity coming from the upstream boundary layer which has not been dissipated. At $x/h = 4.5$, one can observe that the EDDES method ensures a decrease of the eddy viscosity in the reverse-flow region, because the levels of μ_t/μ are once again divided by 4 in comparison with the DDES. As expected, the levels of μ_t remain identical with both methods in the boundary layer developing on the upper plate at the two longitudinal locations.

Finally, the vertical evolution of the ratio u_{rms}/U_∞, where u_{rms} is the resolved averaged fluctuations of u, is represented in Fig. 7 for the stations $x/h = 1.2$ and $x/h = 4.5$.

At $x/h = 1.2$, the ratio u_{rms}/U_∞ predicted by the EDDES computation is in quite good agreement with the experimental data, whereas the DDES computation predicts a maximal value of u_{rms}/U_∞ 3.6 times lower than the one predicted by the experiments. This is consistent with the fact that the turbulent viscosity is much larger in the DDES case than in the EDDES one. It is then possible to imagine that the DDES modeled fluctuations compensate for the lack of a resolved one. Nevertheless, this scheme is not supported by the data obtained at $x/h = 4.5$ where the resolved turbulent fluctuation levels of the DDES case are overestimated by more than 50%. This can be explained by the too large scales coherent structures observed

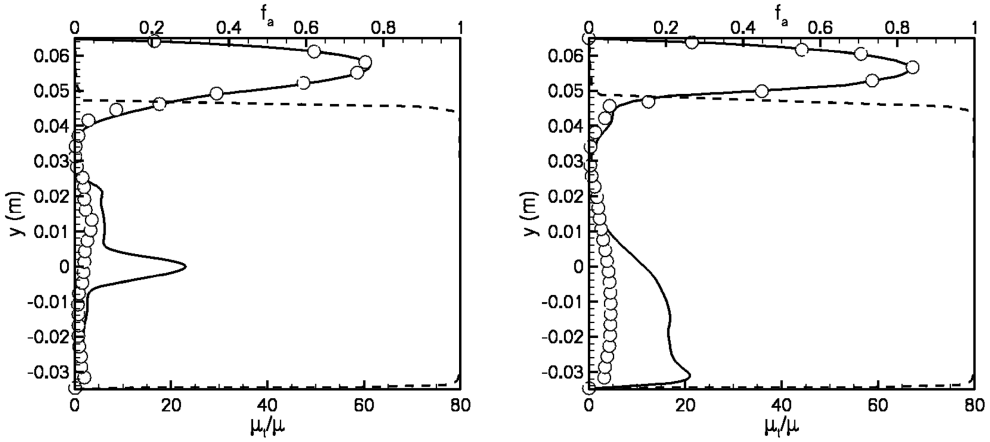

Fig. 6 Evolution of the eddy viscosity at $x/h = 1.2$ (left) and $x/h = 4.5$ (right); dashed lines: f_a, solid lines: DDES; symbols: EDDES.

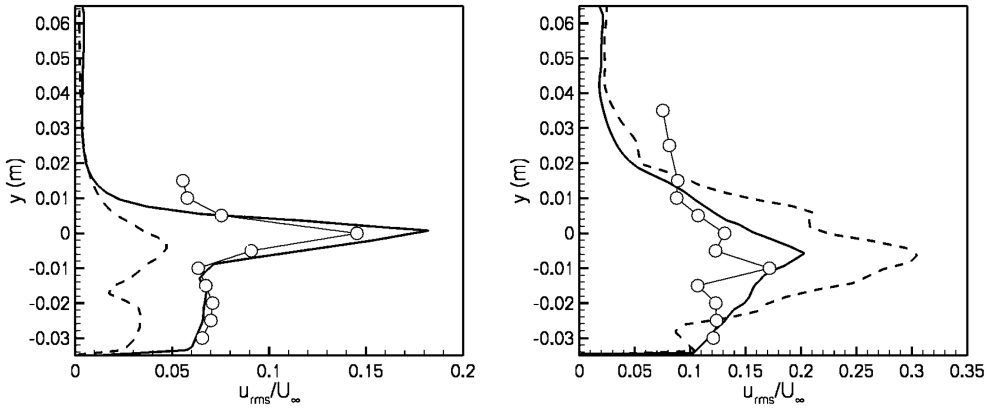

Fig. 7 Evolution of $u_{\mathrm{rms}}/U_\infty$ as a function of d_w. Left: $x/h = 1.2$; right: $x/h = 4.5$; dashed lines: DDES; solid Lines: EDDES; symbols: experiment.

in Fig. 4. At this station, an addition of the modeled turbulence to the resolved one should then increase the discrepancies with respect to the experiments. Conversely, the agreement of the EDDES with the experimental fluctuation levels is satisfactory at $x/h = 4.5$. As a result, one can conclude that the decrease of turbulent viscosity obtained thanks to the EDDES formulation during the early stage of the transition process translates itself to a significant improvement in terms of general result quality. In particular, the EDDES resolved turbulent longitudinal fluctuations are in good agreement with the experimental data.

The next step of the study is to apply this method to the computation of the fully separated flow over a moderately swept missile fin in order to evaluate the ability of the EDDES method to accurately predict separation of the flow and then the aerodynamic loadings.

V. Computation of the Flow Over a Stalled Missile Fin

A. Description of the Configuration

Simulations are performed here on a 50-deg backward swept missile-fin configuration in transonic flow ($M_\infty = 0.7$) at a realistic Reynolds number ($Re_c = 5.8 \times 10^6$) and at an angle of attack $\alpha = 25$ deg. The root chord of the fin is $c = 0.285$ m, its span is 0.19 m, and its relative maximum thickness is 8%. Moreover, this fin is mounted on a vertical plate and a slot of 0.5 mm is present in the experiment between the fin and the vertical plate to permit a measurement of forces and moments in the three directions. Consequently, it has been decided to consider this slot in the computation to fit as much as possible to the experimental configuration.

The geometry is presented in Fig. 8. It is worthwhile to notice that the leading edge of the fin is very sharp.

In the following sections, x_c represents the longitudinal position divided by the root chord c and z_b the transverse position z divided by the local span b.

All of the experimental data presented in this paper were acquired in ONERA's transonic wind tunnel (S3MA) at test conditions of $M_\infty = 0.7$, $P_{i\infty} = 1.5$ bar, and $T_{i\infty} = 278$ K. The fin had been painted with pressure sensitive paint (PSP) which gives access to the distribution of pressure on the suction side. Moreover, aerodynamic loadings and moments have been measured [88].

B. Overview of the RANS Computations

As a starting point of the study, steady RANS computations were first achieved. The computational domain is a half-sphere whose radius is equal to 15 c and it is divided into 16 domains (see Fig. 9). The boundary conditions are given in Fig. 10. A nonslip adiabatic wall condition is applied on the surface of the missile fin and to the vertical plate.

The instantaneous and time-averaged flows in the region in the entire computational domain have been checked and correspond to the required aerodynamic field, meaning that the boundary conditions are adequate. To study the effect of the mesh resolution on the results, three multiblock meshes have been built. Their main characteristics are as follows: $M_1 = 550,000$; $M_2 = 16 \times 10^6$; $M_3 = 21 \times 10^6$. These computations have been carried out using the minmod numerical limiter and with $\Psi = 0.1$. Moreover, a computation using the limiter of Koren and $\Psi = 0.001$ has been carried out on the mesh M_3 to study the effect of a decrease of the numerical dissipation on the solution.

Figure 11 presents the surface mesh on the suction side for the grid M_3. The mesh is significantly refined in the leading-edge vicinity to allow for an accurate description of the shear layer separation. Elsewhere, it is as uniform as possible.

1. Presentation of the Aerodynamic Performances of the Missile Fin Predicted by the Steady RANS Computations

Table 1 gives the aerodynamic performances obtained thanks to the steady RANS computations. Discrepancies with the

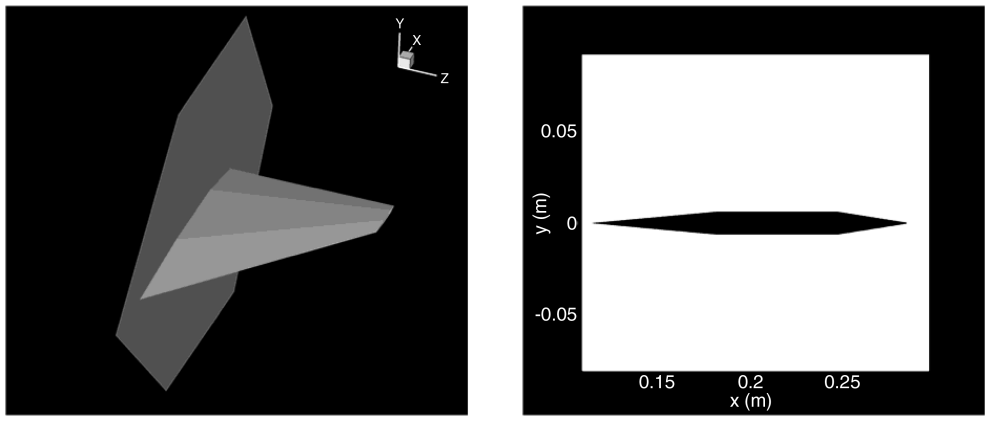

Fig. 8 Geometry of the missile fin. Left: perspective view; right: side view ($z_b = 0.5$).

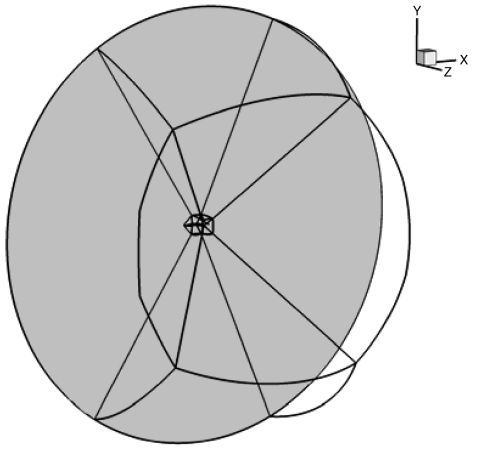

Fig. 9 Computational domain of the missile-fin flow.

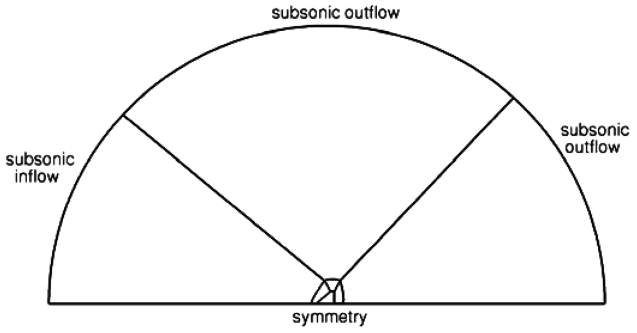

Fig. 10 Boundary conditions.

experimental data are also reported. The computation with the coarser mesh M_1 overestimates the lift coefficient C_L by 17% and underestimates the drag coefficient C_D by about 40%. These discrepancies with the experiments are accentuated by increasing the mesh refinement as illustrated by the results obtained using the mesh M_2. However, results obtained with M_3 are nearly identical to the ones of the intermediate grid. Parallel to this, the decrease of numerical dissipation has no appreciable effect on the aerodynamics performances on the mesh M_3. These observations reveal that the RANS computations are satisfactorily converged on the mesh M_3 and that the differences with the experimental data are only due to modeling errors. Consequently, in the following, all computations are carried out on the grid M_3 with the less dissipative numerical option.

2. Analysis of the Flow Predicted by the RANS Computation

Figure 12 compares the pressure distribution on the suction side obtained with the RANS computation with the PSP data. This figure represents the evolution of K_p [given by Eq. (14)] with the spanwise location z,

$$K_p = \frac{p - p_\infty}{0.5\rho_\infty U_\infty^2} \tag{14}$$

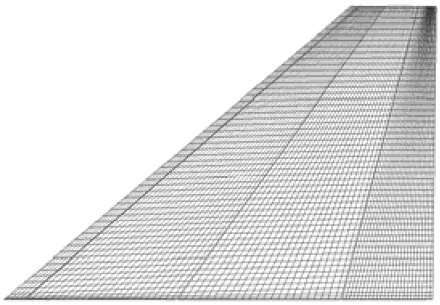

Fig. 11 Surface mesh of the missile fin (mesh M_3, only one point over four is plotted in each direction).

On the first 30% of the chord, the RANS computation overestimates the depression by 150%. Downstream from this position, the computed pressures are in correct agreement with the experimental data.

To analyze the flow more deeply, let us use two probe lines P_1 and P_4, perpendicular to the surface of the fin and whose locations are given in Fig. 13. These two lines are located in the area of minimum pressure. Figure 14 shows the profiles of the longitudinal velocity at these two locations.

At the first probes line P_1, the flow coming from the leading edge rolls up into a large-scale vortex and the streamwise velocity reaches the value of $1.9U_\infty$ in the core of this vortex at $d_w = 0.006$ m. The swirling movement of the leading-edge vortex is illustrated by extreme values of w/U_∞, which reach -1.2 and 2.7. The behavior of the flow is quite different at the probes line P_4. Indeed, the minimum of the velocity ratio u/U_∞ equals -0.005 and a decay of the spanwise velocity is observed. This modification of the velocity profiles illustrates the breakdown of the leading-edge vortex.

These observations confirm that RANS computations predict the presence of a primary vortex up to $x_c = 0.3$. This vortex explains the intense depression observed on the pressure distribution in Fig. 13. Alternatively, one can make use of the analysis of the computation to conjecture that the pressure distribution obtained experimentally is the result of a fully separated flow.

C. Comparison of DDES and EDDES Methods

To correctly predict the physical phenomenon of the stalled flow and then the aerodynamic performances of the missile fin, DDES and EDDES computations have been carried out. For these unsteady computations, the code was used in a time-consistent mode with a time step set equal to 2.6×10^{-7} s. This ensures the convergence of the Newton subiterative process of the implicit Gear scheme with four subiterations. Moreover, the grid M_3 is used because it presents a LES resolution in the region where the flow is separated.

1. Study of the Instantaneous Flow

Figure 15 shows an isosurface of $Q = 400 \times U_\infty^2/c^2$ flooded by the adimensionalized longitudinal vorticity. Significant differences between the EDDES and DDES can be observed on the two instantaneous flows. Although no vortical structures are visible near

Table 1 Effect of the grid refinement and of the numerical dissipation on the prevision of the aerodynamic performances of the fin

Aerodynamic performances	Experimental data	M_1	M_2	M_3	M_3 low dissipation
C_L	0.822	0.963 (+17.1%)	0.99 (+20.5%)	0.996 (+21.2%)	0.995 (+21%)
C_D	0.028	0.0172 (−38.6%)	0.019 (−32.1%)	0.019 (−32.1%)	0.019 (−32.1%)
x_{cp}	0.549	0.511 (−6.9%)	0.521 (−5.1%)	0.522 (−5.1%)	0.523 (−4.9%)
z_{cp}	0.349	0.322 (−7.7%)	0.332 (−5.1%)	0.332 (−5.1%)	0.332 (−5.1%)

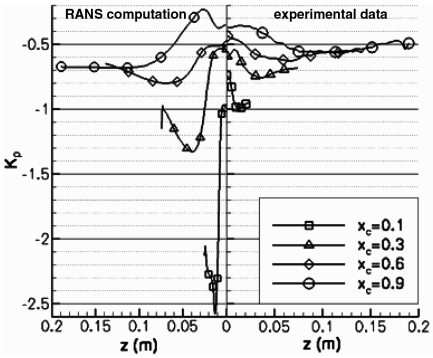

Fig. 12 Distribution of K_p on the suction side as a function of z given by the RANS computation confronted to the experimental data.

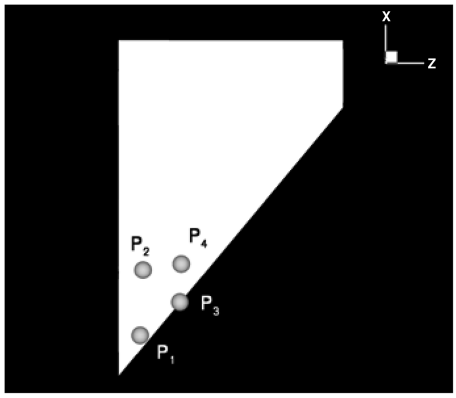

Fig. 13 Position of the four lines probes on the suction side of the fin. P_1: $x_c = 0.15, z_b = 0.95$; P_2: $x_c = 0.35, z_b = 0.25$; P_3: $x_c = 0.25, z_b = 1$; P_4: $x_c = 0.25, z_b = 0.8$.

the apex of the fin in the DDES flow, numerous vortical structures emanating from the leading edge of the missile fin are predicted by the EDDES method in this region.

Another useful way to illustrate the development of flow instabilities is to plot the evolution of the density gradient $\|\text{grad}(\rho)\|$. Figure 16 depicts the contours of this quantity at $z_b = 0.5$.

This figure confirms the previous observation. In fact, the shear layer emanating from the leading edge seems steady in the DDES flow up to $x_c = 0.3$ and the structures due to the Kelvin–Helmholtz instability develop much more quickly in the EDDES computation. The development rate of this instability results from the level of viscosity (numerical + physical) produced by the simulation. With the numerical scheme being the same in the two simulations, one can then anticipate from this figure that the level of turbulent viscosity is smaller in the EDDES simulation than in the DDES one. Farther downstream when these structures have merged, a three-dimensional flow is observed with the two methods.

A similar behavior is observed for the shear layer emanating from the trailing edge (see Fig. 17). Indeed, as observed in Fig. 17, the EDDES method enhances the turbulent activity in this region in comparison with the DDES one.

The first conclusion that can be made from these observations is that the aim of the EDDES is reached in the sense that this method clearly improves the description of the resolved part of the turbulent field.

2. *Study of the Time-Averaged Flow*

The purpose of this section is to present solutions obtained with DDES and EDDES methods and to compare them to the experimental data to highlight their beneficial effects with respect to RANS computations on the time-averaged flow.

After a transient of $6T_c$, where T_c is the time scale defined by $T_c = c/U_\infty$, all the computations were time averaged on a period of $5T_c$.

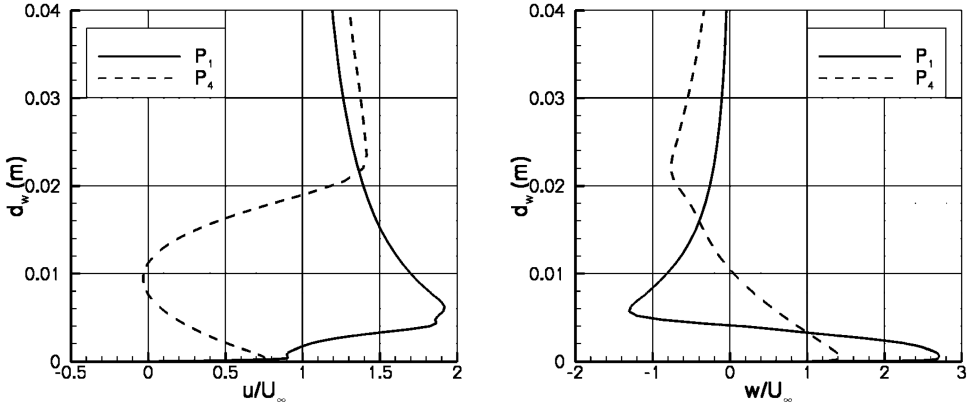

Fig. 14 Evolution of u/U_∞ (left) and w/U_∞ (right) as a function of d_w.

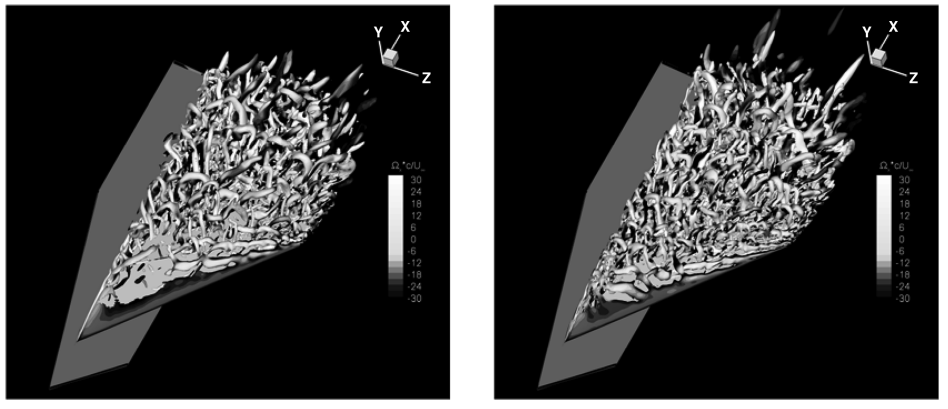

Fig. 15 Visualization of the instantaneous vortical structures predicted by the DDES (left) and the EDDES (right).

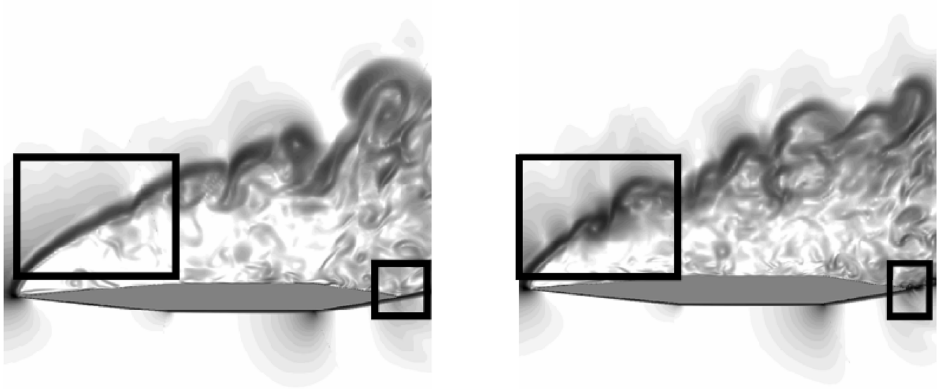

Fig. 16 Contours of $\|\mathbf{grad}(\rho)\|$ at $z_b = 0.5$ predicted by DDES (left) and EDDES (right) computations.

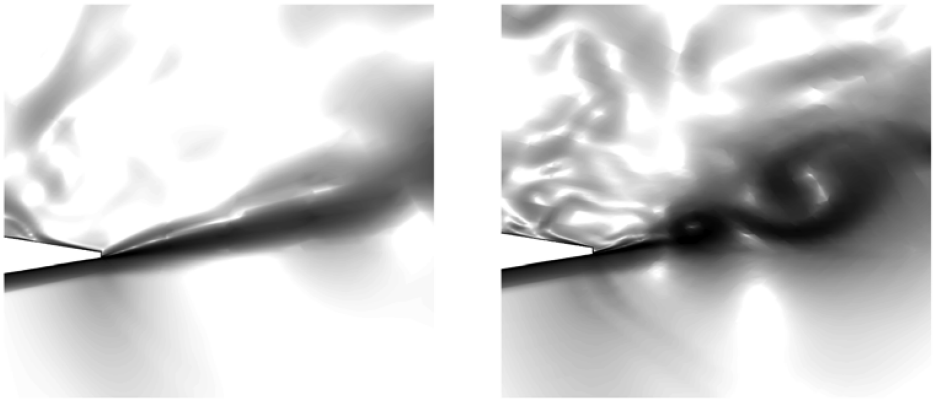

Fig. 17 Contours of $\|\mathbf{grad}(\rho)\|$ at $z_b = 0.5$ predicted by DDES (left) and EDDES (right) computations in the region of the trailing edge of the missile fin.

To get an overview of the time-averaged flow topology obtained with the two methods, Fig. 18 represents the tridimensional streamlines over the suction side of the missile fin. These streamlines are colored by the longitudinal velocity, the white color representing negative values of u and the black color, the positive ones.

This figure highlights a similar flow topology for the two cases. Indeed, one can observe the deviation of the longitudinal flow at the leading edge of the fin and beneath these streamlines, the streamlines roll up, denoting a fully separated flow.

Nonetheless, this figure illustrates a noticeable difference in the flow topology between the two considered cases. In fact, one can clearly observe that the focus point, defined as being the convergence point of the rolling streamlines, is closer to the leading edge in the EDDES computation than in the DDES one, revealing that the flow separation is delayed by the DDES computation. This observation can be associated with the delay in the developments of the instabilities embedded in the shear layer previously observed in the instantaneous DDES flow.

Figure 19 shows profiles of the ratio u/U_∞ as a function of d_w at the four probes lines identified in Fig. 13.

The first observation that can be made is the presence of stagnation or a reverse flow whatever the position with both DDES and EDDES. This contrasts with the RANS computation for which the presence of a leading-edge vortex was predicted. Thus, this represents a significant improvement regarding the RANS results.

However, some differences exist between the time-averaged flows predicted by the DDES and EDDES computations. In fact, at the first position P_1, the reverse flow predicted by the EDDES computation is somewhat higher than the one predicted by the DDES method, as was presented in Fig. 18. Moreover, at the probes line P_2, no reverse flow is visible in the DDES solution whereas u/U_∞ reaches the value of -0.1 at $d_w = 0.02$ in the EDDES time-averaged flow.

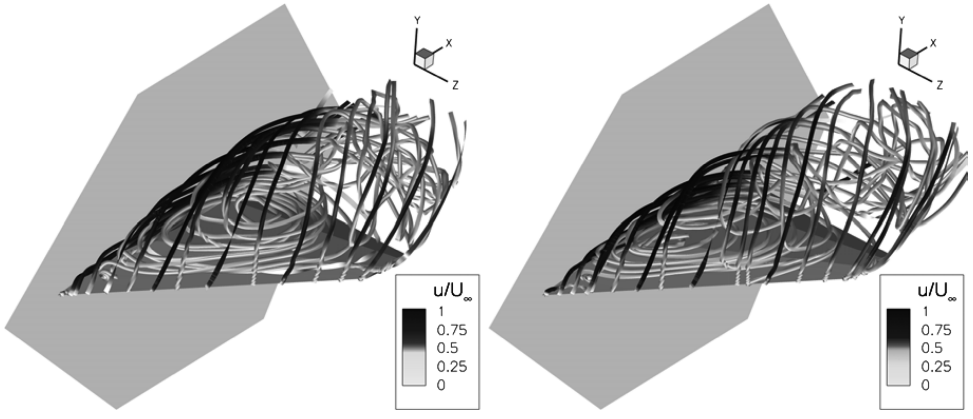

Fig. 18 Visualization of the time-averaged streamlines over the suction side of the missile fin. Left: DDES; right: EDDES.

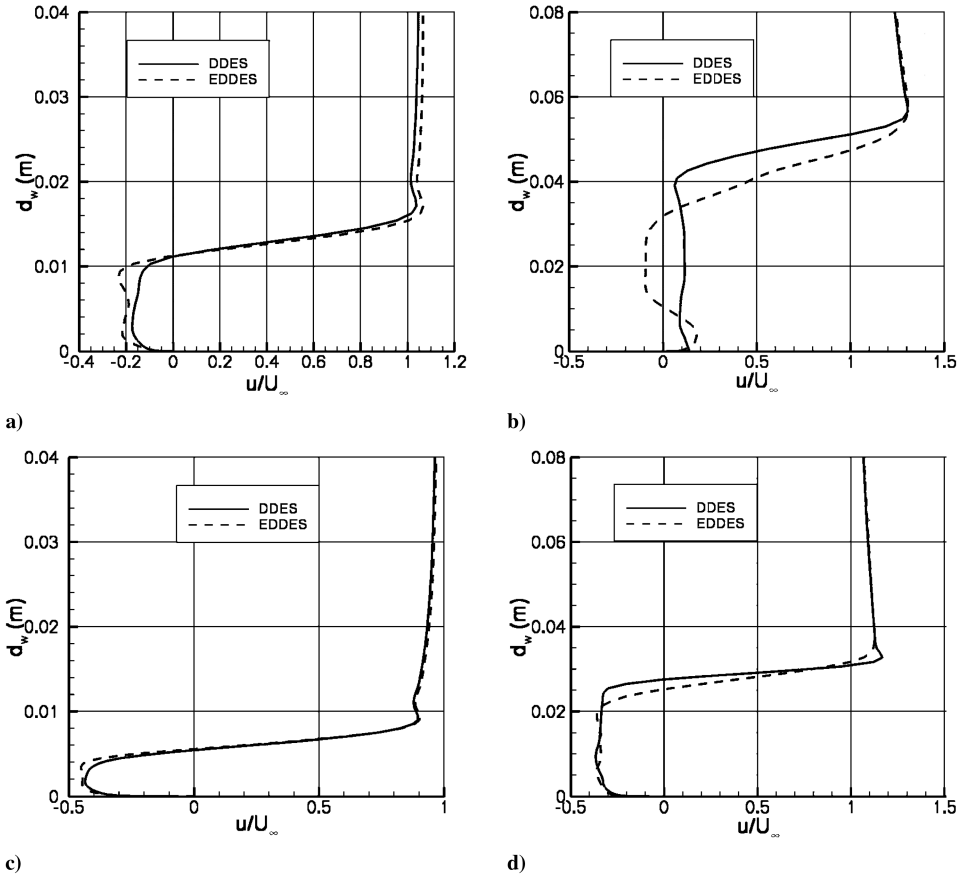

Fig. 19 Evolution of u/U_∞ as a function of d_w. a) P_1; b) P_2; c) P_3; d) P_4.

Despite these observations, the two computations tend to predict a similar evolution of the longitudinal flow near the leading edge of the missile fin. Indeed, in spite of small difference in the intensity, a reverse flow is predicted at the probes lines P_3 and P_4 by the DDES and EDDES methods.

However, these figures not only illustrate differences in the reverse flow, they also underline the effect of the method on the time-averaged flow in the region of the shear layer. Indeed, whatever theposition, extreme values of u/U_∞ and velocity gradients are quitedifferent from the DDES to the EDDES method in the shear layer that may impact the development of the Kelvin–Helmholtz instability.

Thus, both DDES and EDDES predict the separation of the shear layer at the leading edge of the missile fin and a "dead water" region between this shear layer and the surface of the fin. These observations agree well with the experiment of flows over the moderate sweep delta wing at such an incidence (see [18]).

Figure 20 shows the profiles of averaged eddy viscosity given by DDES and EDDES as a function of the distance from the wall d_w at the four previous positions. These probes are close to the leading edge of the missile fin where the flow should be the most sensitive to the numerical method because it is the location where the separation occurs. To identity the location of the RANS/LES switch, the profile of the function f_a is also represented. The profiles are normalized by the local maximum value of the viscosity obtained using DDES.

In all of the station, the profiles of turbulent viscosity are qualitatively similar. They all exhibit one peak of viscosity near the wall and another one in the shear layer.

Figure 20 illustrates the effect of the EDDES method on the eddy viscosity whatever the position considered.

As soon as f_a has reached its threshold value of 0.8, the first peak of eddy viscosity decreases, with a maximum decay at the position P_3 where the ratio $\upsilon_{t\mathrm{DDES}}/\upsilon_{t\mathrm{EDDES}}$ reaches the value of 3.2 at $d_w = 0.001$. For d_w higher than 0.001, both simulations operate in the LES mode, as illustrated by the value $f_a = 1$, and the EDDES method carries on the decrease of the eddy viscosity. The second peak of υ_t is strongly affected by the EDDES model because it is the place where the decay is maximal and the ratio $\upsilon_{t\mathrm{DDES}}/\upsilon_{t\mathrm{EDDES}}$ reaches 5.2 at $d_w = 0.028$ at the probes line P_4.

Thus, the principal effect of the EDDES computation, by comparison with DDES, is the decrease of the second peak of eddy viscosity. The study of the ratio k/U_∞^2, where k is the resolved turbulent kinetic energy illustrates the impact of this decay on the resolved fluctuation levels. Figure 21 shows the evolution of k/U_∞^2 at the four previous positions.

The decay of the eddy viscosity in the LES region allowed by the use of the EDDES method has a significant effect on the levels of resolved turbulent fluctuations. On P_1, P_2, and P_4, the peaks of k/U_∞^2 are nearly multiplied by 3 in the shear layer region. Coupling this observation with the fact the eddy viscosity is decreased using EDDES, it appears clearly that a part of the turbulent spectrum that was modeled in the DDES is now resolved in EDDES. Then, it explains the observations made in the previous section which have highlighted the earlier development of the turbulent structures in the EDDES case.

In this fully separated flow, the switch from RANS to LES mode identified with the function f_a occurs very near the wall and most of the flow is treated in LES mode. This test case is then well suited to demonstrate the interest of EDDES which can be distinguished from DDES only by its behavior in LES mode.

3. Effect of the Numerical Method on the Prediction of the Aerodynamic Performances

Table 2 presents the global aerodynamic performances of the missile fin obtained with the DDES and EDDES computations.

As expected regarding the topology of the flows predicted by these computations, the aerodynamic loadings applied on the missile fin and the position of the aerodynamic center of pressure are better

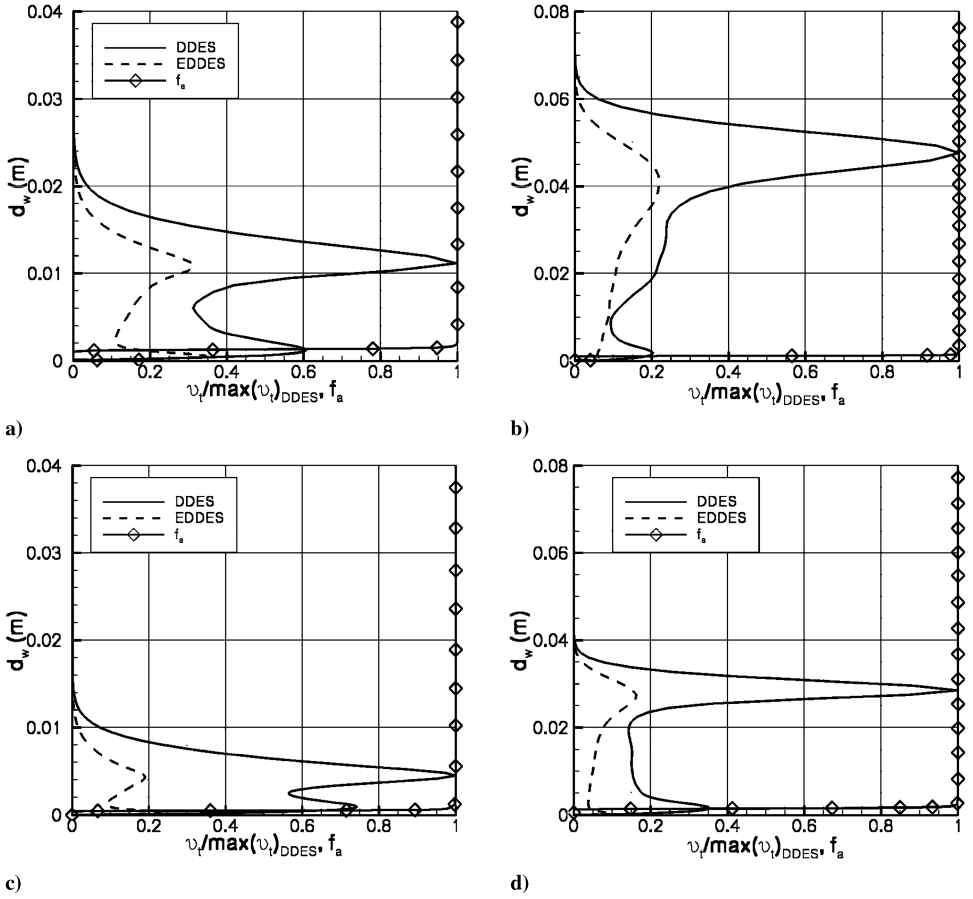

Fig. 20 Evolution of the eddy viscosity and f_a as a function of d_w. a) P_1; b) P_2; c) P_3; d) P_4.

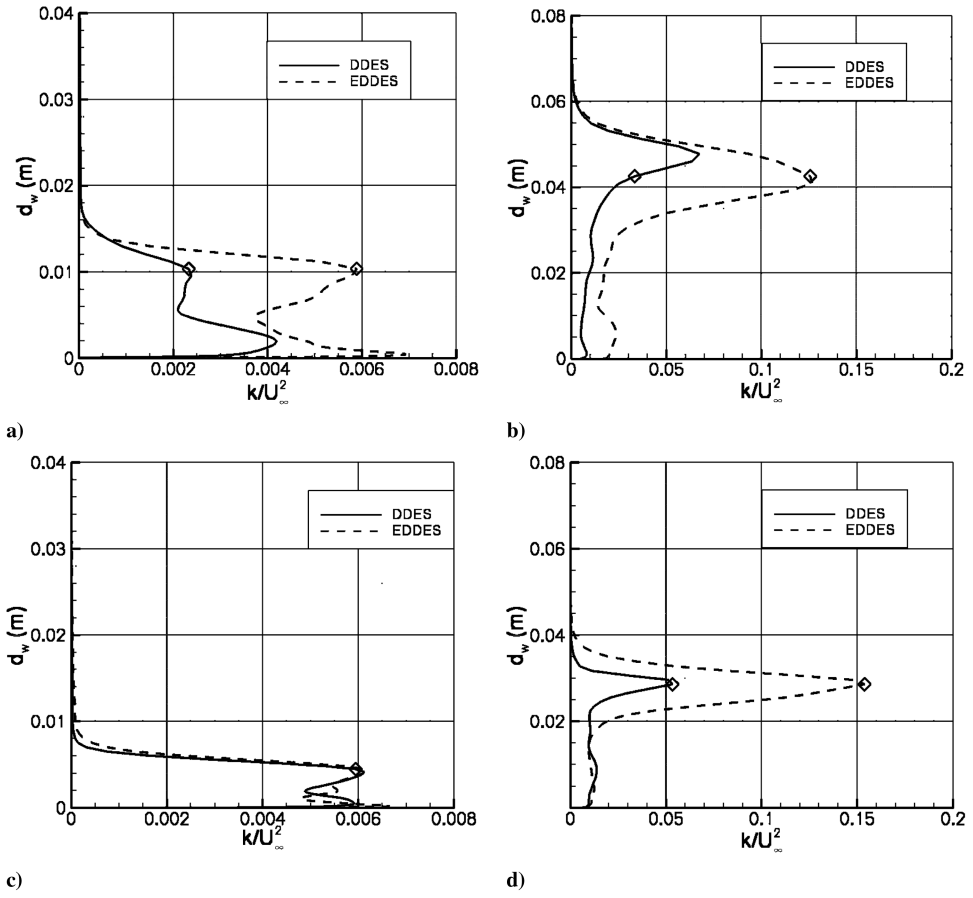

Fig. 21 Evolution of k/U_∞^2 as a function of d_w. a) P_1; b) P_2; c) P_3; d) P_4.

Table 2 Aerodynamic performances predicted by DDES and EDDES computations

Angle of attack	Aerodynamic performances	Experimental data	DDES	EDDES
25 deg	C_L	0.822	0.823 (<0.5%)	0.847 (+3%)
	C_D	0.028	0.0314 (+8.2%)	0.0294 (+1.3%)
	x_{cp}	0.549	0.5626 (+2.4%)	0.5583 (+1.7%)
	z_{cp}	0.349	0.3537 (+1.34%)	0.3523 (+0.94%)

estimated by these current simulations than by the previous RANS computations.

Quantitatively, the DDES computation reduces the error on the lift and drag coefficients to 0.5 and 8.2%, respectively. In the same way, the errors on longitudinal and spanwise positions of the aerodynamic center of pressure are now limited to 2.4 and 1.34%, respectively, with the DDES. This represents a significant improvement with respect to the RANS computation.

In comparison with the DDES, the EDDES computation slightly deteriorates the lift coefficient evaluation. The error remains more than acceptable and reaches only 3%. Furthermore, a great improvement is found concerning the evaluation of C_D with an error level divided by 6.3 with respect to the DDES prediction. It is noteworthy that the pressure drag represents about 87% of the total drag in this case. Additionally, the position of the center of pressure is improved and the small level of error on this quantity permits one to provide the missile manufacturer with a very accurate estimation of the hinge moment on the actuator fin.

The aerodynamic coefficients represent the integral of the pressure forces and can hide strong discrepancies on the distribution of the aerodynamic loads. Thus, the distribution of K_p on the pressure side in the spanwise direction is depicted in Fig. 22. The pressure distributions are nearly identical between both computations whatever the streamwise location. This result is not surprising because the attached flow is solved in the RANS mode in both simulations.

As a consequence, the discrepancies between DDES and EDDES which have been noticed on the aerodynamic coefficients are caused by differences concerning the prediction of K_p on the suction side of the fin. To confirm this postulate, Fig. 23 displays the repartition of K_p as a function of z on the suction side for the DDES and EDDES computations. Comparisons with PSP data are also provided.

The DDES computation underestimates the pressure by 43% at $x_c = 0.1$ and by 27% at $x_c = 0.3$. Oppositely, downstream from this position, the pressure is overestimated and the error reaches the value of 13% at $x_c = 0.6$.

Besides, the use of EDDES allows a decrease of the error to 31% at $x_c = 0.1$. This constitutes progress with respect to DDES but the error remains quite large. It is hoped that it does not contribute much to the integral because it concerns only a small portion of the surface on the fin. Downstream from this location, the prediction of the pressure distribution is in a satisfying agreement with the experimental data and this agreement is generally better with EDDES than with DDES.

As has been shown in this section, the use of the DDES computation leads to a better description of the time-averaged flow in comparison with the RANS model, because a fully separated flow is predicted. This leads to a satisfying prevision of the aerodynamic loadings in a first approach.

The use of the EDDES method leads to a significant diminution of the eddy viscosity in the LES region and then leads to a modification of the time-averaged flow near the wall in comparison with the time-averaged flow predicted by the DDES computation. The consequence is a better prediction of the pressure distribution on the suction side of the missile fin and then an improvement of the prediction of the aerodynamics loadings and of the position of the aerodynamic center of pressure. To conclude this study, the next section is dedicated to the spectral analysis of the flow mostly focused on the region of the shear layer.

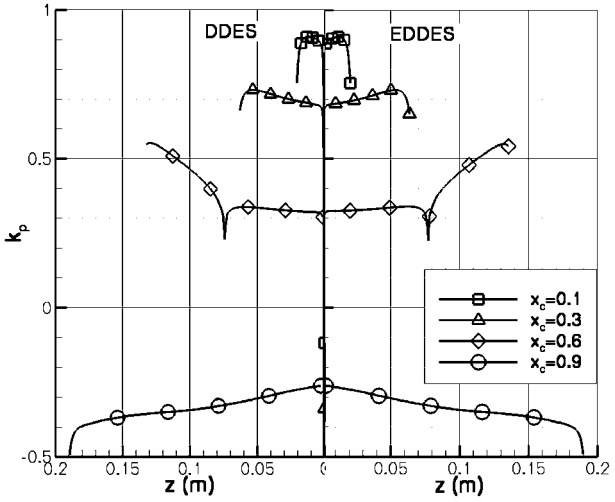

Fig. 22 Repartition of K_p on the pressure side predicted by DDES and EDDES.

4. *Spectral Analysis of the Flow*

The spectral analysis concerns the vertical velocity v registered at positions marked by diamonds in Fig. 21. This analysis has been performed using the method of Welch [89]. The spectral information is averaged on 12 blocks, resulting in a frequency resolution equal to 1 kHz. These spectra are plotted in Fig. 24.

It is obvious from this figure that, whatever the considered position, the EDDES method magnifies the spectral content of the flow, because this method allows an increase of the spectral power

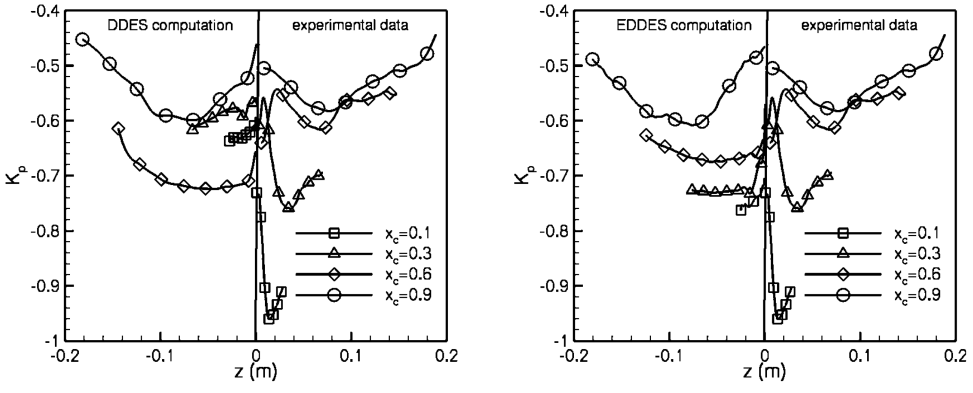

Fig. 23 Repartition of K_p on the suction side predicted by the DDES, EDDES, and experimentation.

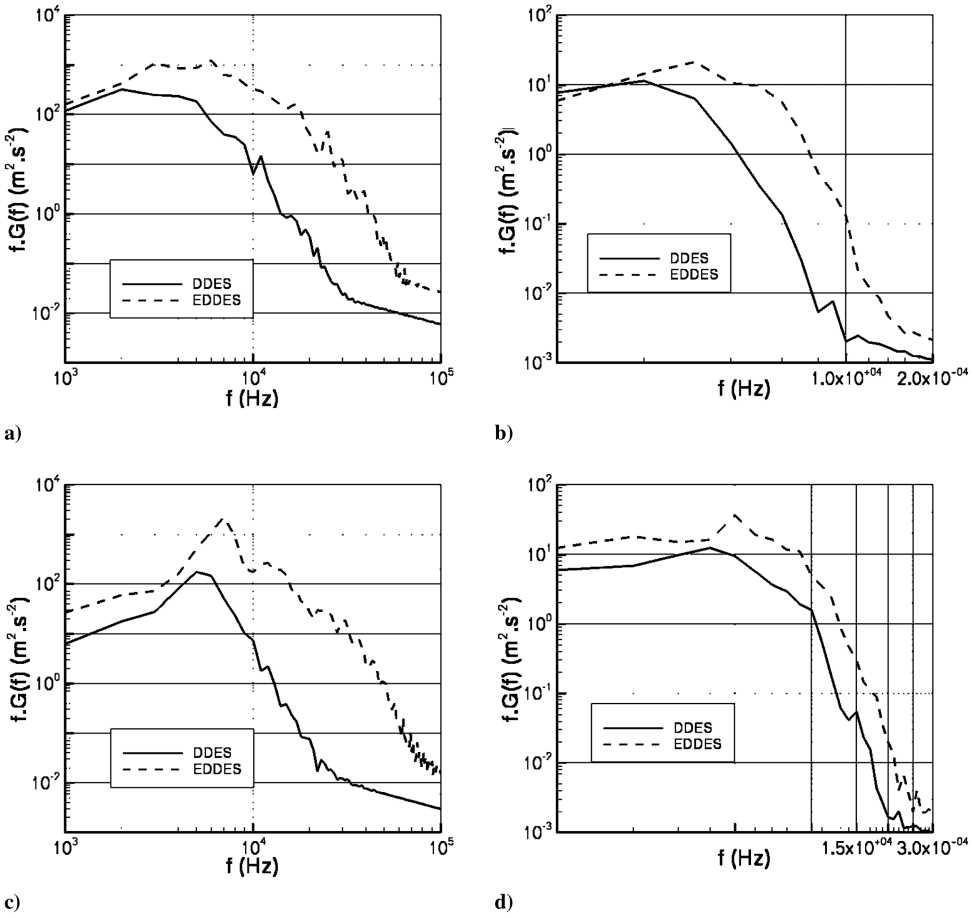

Fig. 24 Vertical velocity spectra from the DDES and EDDES computations. a): P_1; b): P_2; c): P_3; d): P_4.

density for all frequencies present in the signals. This is directly connected with the observations made previously about the improvement in the description of the turbulent structures thanks to the EDDES.

The analysis of the spectrum concerning the EDDES computation at the probe P_1, near the apex of the fin, reveals a low amplitude peak at the frequency $f = 6000$ Hz ($St_c = 7.5$) whereas no peak is discernible in the DDES signal. As illustrated by the spectral analysis at the position P_3, an outward displacement has the consequence of an increase of the privileged frequency. Indeed, peaks around $f = 7000$ Hz ($St_c = 8.8$) and $f = 5000$ Hz ($St_c = 6.3$) are, respectively, observed in the EDDES and DDES spectrum.

An increase of the distance from the leading edge induces a decrease of the privileged frequency as shown in the analysis of the spectrum at P_2 and P_4. Concerning the probe P_2, a decay to $St_c = 2.5$ of the privileged frequency is noticeable in the EDDES spectra and once again, no apparent frequency occurs in the DDES spectra. This general behavior is in agreement with studies of canonical shear layers [90].

Moreover, the increase of frequency with the spanwise position illustrated by the comparison of the spectra at P_2 and P_4 is in agreement with experimental observations of Yaniktepe and Rockwell [19] concerning a 38.7 deg sweep delta wing at $\alpha = 25$ deg for a Reynolds number of $Re_c = 1000$.

The differences in the privileged frequencies, associated with the Kelvin–Helmholtz instability, between the DDES and EDDES method corroborate the previously made observations concerning the development of vortical structures in the shear layer.

The spectral content of the flow is not only magnified in the region of the leading edge by the EDDES method, but also the upper trailing edge ($x_c = 1$, $z_b = 0.5$, $d_w = 0.09$) as shown in Fig. 25.

Once again, the EDDES method increases the power spectra density, whatever the frequency considered. This means that even if the reduction of the eddy viscosity is more significant at the beginning of the shear layer, the use of the EDDES method improves the description of the turbulent flow everywhere in the LES region.

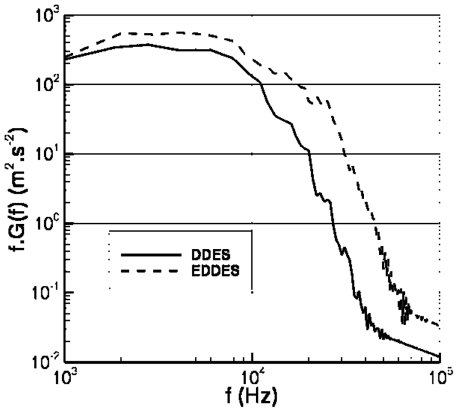

Fig. 25 Spectral analysis of the vertical velocity in the shear layer at $z_b = 0.5$.

VI. Conclusions

An extension of the DDES method combining the best features of the DDES method with the ones of the ZDES method has been presented in this paper. It lies on a modification of the length scale Δ and on the wall-correction functions when the DDES operates in LES mode. This modification results in a faster decay of the eddy viscosity in the LES region.

A first computation of an attached flow allowed validating the EDDES method because a RANS-like behavior has been found as

expected. To validate the method in the case of a fully separated flow, the DDES and EDDES methods have both been used to compute the flow downstream from a backward-facing step for which comprehensive experimental data are available. The EDDES method improves significantly the results with respect to the original DDES. This improvement which is particularly sensitive concerning the turbulent fluctuations has been attributed to the reduction of the eddy viscosity in the early development of the shear layer thanks to the EDDES formulation.

Finally, computations have been carried out in the case of a 50-deg sweep transonic missile fin at the angle of attack of 25 deg. Although RANS computations still predict the presence of the leading-edge vortex over hardly one-third of the missile-fin cord, leading to an significant overestimation of the lift coefficient, the flow predicted by the DDES method is fully separated. This improves significantly the prevision of the aerodynamic performances of the missile fin. Quantitatively, the error on the evaluation of the lift coefficient is reduced to 0.5% whereas the RANS computation overestimates this coefficient by 21%. Moreover, the drag coefficient error decreases from 31% using the RANS model to 8.2% using DDES.

As expected from the formulation of this method, the use of the EDDES computation allows a significant decrease of the eddy viscosity in the LES region. This permits an enhancement of the resolved turbulent fluctuations and then a better prediction of the separation of the flow at the leading edge. The Kelvin–Helmholtz vortices embedded in the shear layer emanating from the leading edge and the turbulent phenomena beneath this shear layer are more energetic in the EDDES flow than in the DDES one.

The enhancement of the LES content of the flow has significant practical consequences on the performance evaluation because the pressure distribution on the suction side, the location of the center of pressure, and the drag coefficient are improved using EDDES. The level of error which was unacceptable from an industrial point of view using RANS has been reduced with EDDES to values which permit accurate dimensioning of the fin actuator (3% error on the lift, about 1% on the drag, and less than 1.5% on the center of pressure location). Moreover, RANS/LES methods give access to the loading fluctuations which are useful information, in particular, when estimating the fluctuating loads on the structure.

Acknowledgments

The authors would like to acknowledge the financial support from DGA, the French Ministry of Defense, and to thank their colleagues Nicolas Bertier and Bruno Sainte-Rose (ONERA, Fundamental and Applied Energetic Department) for providing the grid and the experimental data as well as for their helpful collaboration in the study of the backward-facing step test case.

References

[1] Payne, F. M., Ng, T. T., and Nelson, R. C., "Experimental Study of the Velocity Field on a Delta Wing," AIAA Paper 87-1231, 1987.

[2] Elsayed, M., Scarano, F., and Verhaagen, N. G., "Particle Image Velocimetry of the Flow Over a Slender Delta Wing," AIAA Paper 2007-4451, 2007.

[3] Rusak, Z., and Lamb, D., "Prediction of Vortex Breakdown in Leading-Edge Vortices Above Slender Delta Wings," *Journal of Aircraft*, Vol. 36, No. 4, 1999, pp. 659–667. doi:10.2514/2.2508

[4] Délery, J. M., "Aspects of Vortex Breakdown," *Progress in Aerospace Sciences*, Vol. 30, No. 1, 1994, pp. 1–59. doi:10.1016/0376-0421(94)90002-7

[5] Gordnier, R. E., and Visbal, M. R., "Numerical Simulation of the Unsteady Vortex Structure Over a Delta Wing," AIAA Paper 91-1811, 1991.

[6] Magness, C., Robinson, O., and Rockwell, D., "Instantaneous Topology of the Unsteady Leading-Edge Vortex at High Angle of Attack," *AIAA Journal*, Vol. 31, No. 8, 1993, pp. 1384–1391. doi:10.2514/3.11786

[7] Shan, H., Jiang, L., and Liu, C., "Direct Numerical Simulation of Three-Dimensional Flow Around a Delta Wing," AIAA Paper 2000-0402, 2000.

[8] Morton, S. A., Forsythe, J. R., Mitchell, A. M., and Hajek, D., "DES and RANS Simulations of Delta Wing Vortical Flows," AIAA Paper 2002-0587, 2002.

[9] Visbal, M. R., and Gordnier, R. E., "On the Structure of the Shear Layer Emanating from a Swept Leading Edge at Angle of Attack," AIAA Paper 2003-4016, 2003.

[10] Schiavetta, L. A., Badcock, K. J., and Cummings, R. M., "Comparison of DES and URANS for Unsteady Vortical Flows Over Delta Wings," AIAA Paper 2007-1085, 2007.

[11] Hall, M. G., "A Theory for the Core of a Leading-Edge Vortex," *Journal of Fluid Mechanics*, Vol. 11, 1961, pp. 209–228. doi:10.1017/S0022112061000470

[12] Polhamus, E. C., "A Concept of the Vortex Lift of Sharp-Edged Delta Wings Based on a Leading-Edge-Suction Analogy," NASA TN D-3767, 1966.

[13] Gordnier, R. E., and Visbal, M. R., "Higher-Order Compact Difference Scheme Applied to the Simulation of a Low Sweep Delta Wing Flow," AIAA Paper 2003-026, 2003.

[14] Taylor, G. S., Schnorbus, T., and Gursul, I., "An Investigation of Vortex Flows Over Low Sweep Delta Wings," AIAA Paper 2003-4021, 2003.

[15] Gordnier, R. E., and Visbal, M. R., "Compact Difference Scheme Applied to Simulation of Low-Sweep Delta Wing Flow," *AIAA Journal*, Vol. 43, No. 8, 2005, pp.1744–1752. doi:10.2514/1.5403

[16] Gursul, I., "Review of Unsteady Vortex Flows Over Slender Delta Wings," *Journal of Aircraft*, Vol. 42, No. 2, 2005, pp. 299–319. doi:10.2514/1.5269

[17] Ol, M. V., and Gharib, M., "The Passage Toward Stall of Nonslender Delta Wings at Low Reynolds Number," AIAA Paper 2001-2843, 2001.

[18] Ol, M. V., and Gharib, M., "Leading-Edge Vortex Structure of Nonslender Delta Wings at Low Reynolds Number," *AIAA Journal*, Vol. 41, No. 1, 2003, pp. 16–26. doi:10.2514/2.1930

[19] Yaniktepe, B., and Rockwell, D., "Flow Structure on a Delta Wing of Low Sweep Angle," *AIAA Journal*, Vol. 42, No. 3, 2004, pp. 513–523. doi:10.2514/1.1207

[20] Reynolds, G. A., and Abtahi, A. A., "Three-Dimensional Vortex Development, Breakdown and Control," AIAA Paper 89-0998, 1989.

[21] Lowson, M. V., Riley, A. J., and Swales, C., "Flow Structure Over Delta Wings," AIAA Paper 95-0586, 1995.

[22] Payne, F. M., Ng, T. T., Nelson, R. C., and Schiff, L. B., "Visualization and Wake Surveys of Vortical Flow Over a Delta Wing," *AIAA Journal*, Vol. 26, No. 2, 1988, pp. 137–143. doi:10.2514/3.9864.

[23] Riley, A. J., and Lowson, M. V., "Development of a Three-Dimensional Free Shear Layer," *Journal of Fluid Mechanics*, Vol. 369, Aug. 1998, pp. 49–89.

[24] Washburn, A. E., and Visser, K. D., "Evolution of Vortical Substructures in the Shear Layer of Delta Wings," AIAA Paper 94-2317, 1994.

[25] Mitchell, A. M., and Molton, P., "Vortical Substructures in the Shear Layers Forming Leading Edge Vortices," *AIAA Journal*, Vol. 40, No. 8, 2002, pp. 1689–1692. doi:10.2514/2.1844

[26] Erickson, G. E., Schreiner, J. A., and Rogers, L. W., "Multiple Vortex and Shock Interactions at Subsonic, Transonic and Supersonic Speeds," AIAA Paper 90-3023, 1990.

[27] Visbal, M. R., and Gordnier, R. E., "Compressibility Effects on Vortex Breakdown Onset Above a 75-Degree Sweep Delta Wing," *Journal of Aircraft*, Vol. 32, No. 6, 1995, pp. 1359–1366. doi:10.2514/3.46886

[28] Kandil, O. A., Kandil, H. A., and Liu, C. H., "Supersonic Vortex Breakdown Over a Delta Wing In Transonic Flow," AIAA Paper 93-2973, 1993.

[29] Kandil, O. A., Kandil, H. A., and Liu, C. H., "Shock-Vortex Interaction Over a 65-Degree Delta Wing in Transonic Flow," AIAA Paper 93-2973, 1993.

[30] Longo, J. M. A., "Compressible Inviscid Vortex Flow of a Sharp Edge Delta Wing," *AIAA Journal*, Vol. 33, No. 4, 1995, pp. 680–687. doi:10.2514/3.12631

[31] Erickson, G. E., and Rogers, L. W., "Experimental Study of the Vortex Flow Behaviour on a Generic Fighter Wing at Subsonic and Transonic Speeds," AIAA Paper 87-1262, 1987.

[32] Donohoe, S. R., Houtman, E. M., and Bannink, W. J., "Surface Reflective Visualization System Study to Vortical Flow Over Delta Wings," *Journal of Aircraft*, Vol. 32, No. 6, 1995, pp. 1359–1366. doi:10.2514/3.46886

[33] Donohoe, S. R., and Bannink, W. J., "Surface Reflective Visualizations of Shock-Wave/Vortex Interactions Above a Delta Wing," *AIAA Journal*, Vol. 35, No. 10, 1997, pp. 1568–1573. doi:10.2514/2.12

[34] Papamoschou, D., and Roshko, A., "The Compressible Turbulent Shear Layer: An Experimental Study," *Journal of Fluid Mechanics*, Vol. 197, 1988, pp. 453–477. doi:10.1017/S0022112088003325

[35] Goebel, S. G., and Dutton, J. C., "Experimental Study of Compressible Turbulent Mixing Layers," *AIAA Journal*, Vol. 29, 1991, pp. 538–546. doi:10.2514/3.10617

[36] Hall, J. L., Dimotakis, P. E., and Rosemann, H., "Experiments in Nonreacting Compressible Shear Layer," *AIAA Journal*, Vol. 31, No. 12, 1993, pp. 2247–2254. doi:10.2514/3.11922

[37] Clemens, N. T., and Mungal, M. G., "Large-Structure and Entrainment in the Supersonic Mixing Layer," *Journal of Fluid Mechanics*, Vol. 284, 1995, pp. 171–216. doi:10.1017/S0022112095000310

[38] Sarkar, S., "The Stabilizing Effect of Compressibility in Turbulent Shear Flows," *Journal of Fluid Mechanics*, Vol. 282, 1995, pp. 163–186. doi:10.1017/S0022112095000085

[39] Freund, J. B., Lele, S. K., and Moin, P., "Direct Numerical Simulation of a Supersonic Round Turbulent Shear Layer," AIAA Paper 1997-760, 1997.

[40] Clemens, N. T., and Mungal, M. G., "Two- and Three-Dimensional Effects in the Supersonic Mixing Layer," *AIAA Journal*, Vol. 30, No. 4, 1992, pp. 973–981. doi:10.2514/3.11016

[41] Rossman, T., Mungal, M. G., and Hanson, R. K., "Evolution and Growth of Large-Scale Structures in High Compressibility Mixing Layers," *Journal of Turbulence*, Vol. 3, No. 19, 2002, pp. 1–19.

[42] Visbal, M. R., and Gordnier, R. E., "On the Structure of the Shear Layer Emanating from a Swept Leading Edge at Angle Of Attack," AIAA Paper 2003-4016, 2003.

[43] Shan, H., Jiang, L., and Liu, C., "Direct Numerical Simulation of Three-Dimensional Flow Around a Delta Wing," AIAA Paper 2000-042, 2000.

[44] Gornier, R. E., and Visbal, M. R., "Higher-Order Compact Difference Scheme Applied to the Simulation of a Low Sweep Delta Wing Flow," AIAA Paper 2003-0620, 2003.

[45] Gordnier, R. E., and Visbal, M. R., "Compact Difference Scheme Applied to Simulation of Low Sweep Delta Wing Flow," *AIAA Journal*, Vol. 43, No. 8, 2005, pp. 1744–1752. doi:10.2514/1.5403

[46] Mary, I., "Large Eddy Simulation of Vortex Breakdown Behind a Delta Wing," *International Journal of Heat and Fluid Flow*, Vol. 24, No. 4, 2003, pp. 596–605. doi:10.1016/S0142-727X(03)00053-5

[47] Gordnier, R. E., "Computational Study of a Turbulent Delta Wing Flowfield Using Two-Equation Turbulence Models," AIAA Paper 96-2076, 1996.

[48] Brandsma, F. J., Kok, J. C., Dol, H. S., and Elsenaar, A., "Leading Edge Vortex Flow Computations and Comparison with DNW-HST Wind Tunnel Data," NATO RTO/AVT, 2001.

[49] Morton, S. A., Forsythe, J. R., Mitchell, A. M., and Hajek, D., "Detached Eddy Simulation and Reynolds Averaged Navier-Stokes Simulations of Delta Wing Vortical Flow Fields," *Journal of Fluids Engineering*, Vol. 124, 2002, pp. 924–932. doi:10.1115/1.1517570

[50] Morton, S. A., Forsythe, J. R., Mitchell, A. M., and Hajek, D., "DES and RANS Simulations of Delta Wing Vortical Flows," AIAA Paper 2002-0587, 2002.

[51] Sagaut, P., Deck, S., and Terracol, M., *Multiscale and Multiresolution Approaches in Turbulence*, Imperial College Press, London, 2006.

[52] Spalart, P. R., Jou, W. H., Strelets, M., and Allmaras, S. R., "Comments on the Feasibility of LES for Wings, and on a Hybrid RANS/LES Approach," *Proceedings of the 1st AFSOR International Conference on DNS/LES*, Greyden Press, Columbus, OH, 1998, pp. 137–147.

[53] Deck, S., "Zonal-Detached Eddy Simulation of the Flow Around a High Lift Configuration," *AIAA Journal*, Vol. 43, No. 11, 2005, pp.2372–2384. doi:10.2514/1.16810

[54] Spalart, P. R., Deck, S., Shur, M. L., Squires, K. D., Strelets, M. K., and Travin, A., "A New Version of Detached-Eddy Simulation, Resistant to Ambiguous Grid Densities," *Theoretical and Computational Fluid Dynamics*, Vol. 20, 2006, pp. 181–195. doi:10.1007/s00162-006-0015-0

[55] Pechier, M., "Prévisions Numériques de l'effet Magnus pour des Configurations de Munition," Ph.D. Thesis, University Paris 6, Paris, France, 1999.

[56] Roe, P. L., "Approximate Riemann Solvers, Parameter Vectors and Difference Schemes," *Journal of Computational Physics*, Vol. 43, No. 2, 1981, pp. 357–372. doi:10.1016/0021-9991(81)90128-5

[57] Harten, A., "High Resolution Scheme for Hyperbolic Conservations Laws," *Journal of Computational Physics*, Vol. 49, 1983, pp. 357–393. doi:10.1016/0021-9991(83)90136-5

[58] Koren, B., "A Robust Discretisation Method for Advection, Diffusion and Sources Terms," *Numerical Methods for Advection-Diffusion Problems*, edited by C. B. Vreugdenhill and B. Koren, Vieweg, Braunschweig, 1993, pp. 117–137.

[59] Gear, C. W., "Algorithm 407-DIFSUB for the Solution of Ordinary Differential Equations," *Communications of the ACM*, Vol. 14, No. 3, 1971, pp. 185–190. doi:10.1145/362566.362573

[60] Mary, I., and Sagaut, P., "Large Eddy Simulation of the Flow Around an Airfoil Near Stall," *AIAA Journal*, Vol. 40, No. 6, 2002, pp. 1139–1146. doi:10.2514/2.1763

[61] Deck, S., Garnier, E., and Guillen, P., "Turbulence Modeling Applied to Space Launcher Configurations," *Journal of Turbulence*, Vol. 3, No. 57, 2002, pp. 1–21.

[62] Deck, S., and Thorigny, P., "Unsteadiness of an Axisymmetric Separating-Reattaching Flow: Numerical Investigation," *Physics of Fluids*, Vol. 19, No. 065103, 2007, pp. 1–20.

[63] Simon, F., Deck, S., Guillen, P., Sagaut, P., and Merlen, A., "Numerical Simulation of the Compressible Mixing Layer Past an Axisymmetric Trailing Edge," *Journal of Fluid Mechanics*, Vol. 591, 2007, pp. 215–253. doi:10.1017/S0022112007008129

[64] Larchevêque, L., Labbé, O., Mary, I., and Sagaut, P., "LES of a Compressible Flow Past a Deep Cavity," *Physics of Fluids*, Vol. 15, No. 1, 2003, pp. 193–210. doi:10.1063/1.1522379

[65] Dandois, J., Garnier, E., and Sagaut, P., "Unsteady Simulation of Synthetic Jet in a Crossflow," *AIAA Journal*, Vol. 44, No. 2, 2006, pp. 225–238. doi:10.2514/1.13462

[66] Dandois, J., Garnier, E., and Sagaut, P., "DNS/LES of Active Separation Control," *Journal of Fluid Mechanics*, Vol. 574, 2007, pp. 25–58. doi:10.1017/S0022112006003995

[67] Spalart, P. R., and Allmaras, S. R., "A One-Equation Turbulence Model for Aerodynamic Flows," AIAA Paper 1992-04339, 1992.

[68] Catris, S., "Etude de Contraintes et Qualification de Modèles à Viscosité Turbulente," Ph.D. Thesis, SUPAERO, Toulouse, France, 1999.

[69] Deck, S., Duveau, P., d'Espiney, P., and Guillen, P., "Development and Application of Spalart Allmaras One Equation Turbulence Model to Three-Dimensional Supersonic Complex Configurations," *Aerospace Science and Technology*, Vol. 6, No. 3, 2002, pp. 171–183. doi:10.1016/S1270-9638(02)01148-3

[70] Travin, A., Shur, M., Spalart, P. R., and Strelets, M., "Detached Eddy Simulation Past a Circular Cylinder," *Flow Turbulence and Combustion*, Vol. 63, No. 1, 2000, pp. 293–313. doi:10.1023/A:1009901401183

[71] Smagorinsky, J., "General Circulation Experiments with the Primitive Equations," *Monthly Weather Review*, Vol. 91, No. 3, 1963, pp. 99–164. doi:10.1175/1520-0493(1963)091<0099:GCEWTP>2.3.CO;2

[72] Görtz, S., "Realistic Simulations of Delta Wing Aerodynamics Using Novel CFD Methods," Ph.D. Thesis, Royal Institut of Technology (KTH), Stockholm Sweden, 2005.

[73] Görtz, S., and Le Moigne, Y., "Time Accurate Detached Eddy Simulations of a Full Span Delta Wing at High Incidence," AIAA Paper 2003-4216, 2003.

[74] Görtz, S., "Detached-Eddy Simulation of a Full-Span Delta Wing at High Incidence," AIAA Paper 2003-4216, 2003.

[75] Mitchell, A. M., Morton, S. A., and Forsythe, J. R., "Analysis of Delta Wing Substructures Using Detached-Eddy Simulation," AIAA Paper 2002-2968, 2002.

[76] Mitchell, A. M., "Caractérisation et Contrôle de l'éclatement Tourbillonnaire sur une aile delta aux hautes Incidence," Ph.D. Thesis, University of Paris 6, Paris, France, 2000.

[77] Menter, F., Kuntz, M., and Bender, R., "A Scale-Adaptive Simulation Model for Turbulent Flow Predictions," AIAA Paper 03-0767, 2003.

[78] Deck, S., "Numerical Simulation of Transonic Buffet Over a Supercritical Airfoil," *AIAA Journal*, Vol. 43, No. 7, 2005, pp. 1556–1566.
doi:10.2514/1.9885

[79] Trapier, S., Deck, S., and Duveau, P., "Delayed Detached-Eddy Simulation and Analysis of Supersonic Inlet Buzz," *AIAA Journal*, Vol. 46, No. 1, 2008, pp. 118–203.
doi:10.2514/1.32187

[80] Chauvet, N., Deck, S., and Jacquin, L., "Zonal Detached Eddy Simulation of a Controlled Propulsive Jet," *AIAA Journal*, Vol. 45, No. 10, 2007, pp. 2458–2473.
doi:10.2514/1.28562

[81] Breuer, M., Jovicic, N., and Mazaev, K., "Comparison of DES, RANS and LES for the Separated Flow Around a Flat Plate at High Incidence," *International Journal for Numerical Methods in Fluids*, Vol. 41, No. 4, 2003, pp. 357–388.
doi:10.1002/fld.445

[82] Deck, S., "Delayed Detached-Eddy Simulation of self-Sustained Unsteadiness and Side-Loads in an Over Expanded Nozzle" (unpublished).

[83] Magre, P., Collin, G., and Bouchardy, P., "Application de la DRASC l'opération A3C," ONERA Rept. RTS4/3608EY, 1992.

[84] Sabel'nikov, V., and Grisch, F., "Instabilities and Structure of Turbulent Premixed Flame in a Lean Stepped Combustor," ONERA TP 2006-50, 2005.

[85] Moreau, P., Labbe, J., Dupoirieux, F., and Borghi, R., "Experimental and Numerical Study of a Turbulent Recirculation Zone with Combustion," *5th Symposium on Turbulent Shear Flow*, ONERA TP 1985-89, 1985.

[86] Sainte-Rose, B., Bertier, N., Deck, S. and Dupoirieux, F., "Delayed Detached Eddy Simulation of a Premixed Methane Air Flame Behind a Backward Facing Step," AIAA Paper 08-5134, 2008.

[87] Jeong, J., and Hussain, F., "On the Identification of a Vortex," *Journal of Fluid Mechanics*, Vol. 285, 1995, pp. 69–94.
doi:10.1017/S0022112095000462

[88] Fargier, T., "Essai de pesées et de Mesure PSP sur la Gouverne MATRA n° 11E1 dans la veine Transsonique de la Soufflerie S3MA," ONERA Rept. PV 259/06645, 2003.

[89] Welch, P. D., "The Use of Fast Fourier Transform for the Estimation of Power Spectra: A Method Based on Time Averaging Over Short Modified Periodograms," *IEEE Transactions on Audio and Electroacoustics*, Vol. 15, No. 2, 1967, pp. 70–73.
doi:10.1109/TAU.1967.1161901

[90] Ho, C. M., and Huerre, P., "Perturbated Free Shear Layer," *Annual Review of Fluid Mechanics*, Vol. 16, 1984, pp. 365–424.
doi:10.1146/annurev.fl.16.010184.002053

M. Glauser
Associate Editor